JGR Earth Surface

RESEARCH ARTICLE
10.1029/2021JF006502

Special Section:
The Arctic: An AGU Joint Special Collection

Permafrost Thermal Dynamics and Cryostratigraphy at Villum Research Station, Station Nord, Eastern North Greenland (81°N)

S. M. Strand[1,2], H. H. Christiansen[1], and G. L. Gilbert[1,3]

[1]Department of Arctic Geology, The University Centre in Svalbard, Longyearbyen, Norway, [2]Department of Geosciences, University of Oslo, Oslo, Norway, [3]Natural Hazards Market Area, Norwegian Geotechnical Institute, Oslo, Norway

Key Points:

- The presented permafrost thermal record is the second northernmost in the Arctic and reveals the warmest known permafrost north of 80°N
- The warming rate at 20 m depth was 0.07°C/year and 0.05°C/year at the two sites from 2014 to 2021 despite thick and long-lasting snow cover
- Epigenetic permafrost grew into sands and gravels deposited during deglaciation and isostatic emergence of the Prinsesse Ingeborg Halvø

Correspondence to:
S. M. Strand,
sarah.strand@unis.no

Citation:
Strand, S. M., Christiansen, H. H., & Gilbert, G. L. (2022). Permafrost thermal dynamics and cryostratigraphy at Villum Research Station, Station Nord, eastern North Greenland (81°N). *Journal of Geophysical Research: Earth Surface*, *127*, e2021JF006502. https://doi.org/10.1029/2021JF006502

Received 29 OCT 2021
Accepted 14 MAR 2022

Abstract We provide the northernmost permafrost thermal analysis in Greenland through the ground temperature time series (2014–2021) and cryostratigraphy of two 20-m deep boreholes (SN1 and SN2) at Villum Research Station, Station Nord (81°N). Three sedimentary units are identified in the stratigraphy: glacial, glaciomarine, and beach deposits. These sandy and gravelly deposits are interpreted to comprise a deglaciation and isostatic emergence sequence. Ice-poor epigenetic permafrost grew downwards into the deposits following subaerial exposure. Relatively high salinity values (up to 70 ppt) are observed in the glaciomarine unit, resulting in freezing point depressions between 0 and −4°C. The Prinsesse Ingeborg Halvø study area has a polar tundra climate and is unique compared to other high Arctic areas because of a thick (>1 m), long-lasting snow cover. This snow cover results in relatively high permafrost temperatures for the climate and latitude and the warmest known permafrost north of 80°N. Over the seven-year study period, average 20 m permafrost temperature was −7.87°C at SN1 and −7.06°C at SN2. The warming rate at 20 m depth was 0.07°C/year at SN1 and 0.05°C/year at SN2, rates which are similar to those of other high Arctic sites. Active layer thickness, extrapolated from the temperature measurements, varied between 0.5 and 1.16 m. The interplay between snow dynamics and seasonal air temperature controls ground thermal regime in the study area. Air temperatures during autumn and midwinter, the fastest warming seasons, influence the ground thermal regime through the gradually developing, dense snowpack.

Plain Language Summary Permafrost, ground that is frozen for at least two consecutive years, is commonly found in high mountains and polar environments. Permafrost samples and long-term permafrost temperature records are necessary to fully understand permafrost and how it is changing with a warming climate. We present results of permafrost research from Villum Research Station at Station Nord, the northernmost permafrost monitoring site in Greenland and second northernmost worldwide. We collected core samples from two different 20-m deep boreholes and measured temperature in the boreholes for over seven years to understand the permafrost's physical and thermal properties, and how the permafrost reacts to the weather and climate. The permafrost began to form more than 8,000 years ago, after the study area was deglaciated and the sea level lowered. A major reason this permafrost is warmer than other sites in the high Arctic is because the area has more than 1 m of snow in the winter, which is unusual for the polar tundra and acts as an insulating layer. Permafrost at 20 m depth has warmed 0.05–0.07°C per year from 2014 to 2021; these rates are similar to those at other high Arctic sites.

1. Introduction

Permafrost is widespread in the periglacial terrestrial Arctic. The thermal state of permafrost and active layer thickness (ALT) are key indicators for monitoring permafrost as an essential climate variable, designated by the Global Climate Observing System (Global Climate Observing System, 2021). Evaluating permafrost change is important given present and predicted Arctic warming and the central role of permafrost in Arctic terrestrial environments (IPCC, 2021). The permafrost thermal regime is dependent on climate, substrate, specifically lithology and ground ice content, and surface conditions including snow cover, hydrology, and vegetation.

In situ measurements are necessary to characterize the ground thermal regime, and detailed field studies are required to develop a process-based understanding of ground thermal regime development and dynamics. In the high Arctic, in situ permafrost measurements are sparse; in all of northern Greenland, only three sites are

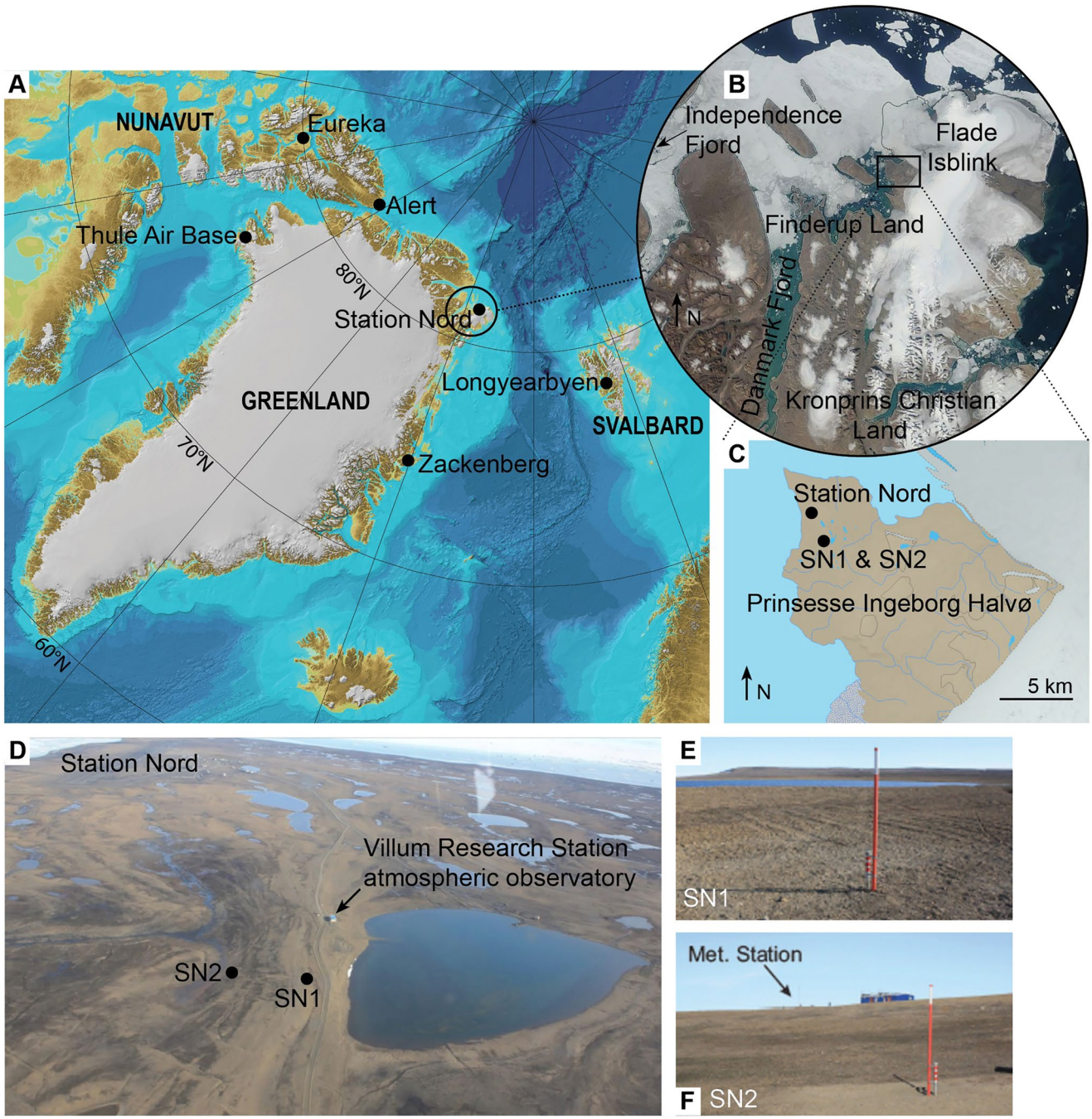

Figure 1. (a) Overview map (base map by Jakobsson et al., 2012) with a black circle designating Kronprins Christian Land and parts of the Independence-Danmark Fjord system in eastern North Greenland. Other permafrost borehole locations discussed in this study are also marked. (b) Terra/MODIS corrected reflectance (true color) satellite image from 30 July 2019 showing Kronprins Christian Land and neighboring regions with typical late-summer sea ice conditions (image acquired through NASA Worldview, https://worldview.earthdata.nasa.gov/). The black box marks the Prinsesse Ingeborg Halvø. (c) Geological Survey of Denmark and Greenland (GEUS) topographic map of the Prinsesse Ingeborg Halvø (map available at http://www.greenmin.gl/). (d) Oblique aerial photo of the study area on the northern tip of the Prinsesse Ingeborg Halvø in August 2014, looking north. (e) SN1. (f) SN2.

instrumented to monitor permafrost conditions: Zackenberg (74°N), Thule Airbase (76°N), and Station Nord (81°N) (Global Terrestrial Network for Permafrost, 2021; Figure 1).

Given the absence of measurement sites, little is known about the ground thermal regime and its variability in northern Greenland, which includes the northernmost land on Earth. No previous studies have focused on the

permafrost ground thermal regime in northern Greenland. A past study by Schomacker et al. (2017) presented four years of air, surface, and 20 cm active layer temperature measurements from Bliss Bugt and Moore Gletscher (both 83°N), which are located approximately 270 km northwest of Station Nord. Ground temperature profiles from Thule Air Base are available in geotechnical reports related to the runway and taxiways (Bjella, 2013, 2015), but no long-term record or ground thermal regime analysis has been published. Permafrost at Zackenberg, ca. 800 km south of Station Nord, is better studied (Christiansen et al., 2008), but recent research has focused on cryostratigraphy (Cable et al., 2018; Gilbert et al., 2017) and permafrost modeling (Rasmussen et al., 2018; Westermann et al., 2015) more than the thermal regime. In high-Arctic Canada, there are two long-term permafrost thermal monitoring sites at Eureka (80°N) and Alert (83°N) on Ellesmere Island (Smith et al., 2010, 2021).

This study is based on data from two boreholes located at Station Nord (81°36' N, 16°40' W), the Danish military outpost, where Aarhus University operates Villum Research Station (VRS). The station is on the Prinsesse Ingeborg Halvø (Princess Ingeborg Peninsula) of Kronprins Christian Land, in eastern North Greenland (Figure 1). Two 20-m deep boreholes were drilled in August 2014 in collaboration with the University Centre in Svalbard (UNIS), establishing VRS permafrost monitoring activities. The permafrost borehole temperature measurements are a permanent component of the VRS climate monitoring program. Ozone and gaseous elemental mercury have been measured at Station Nord since 1996 and 1999, respectively (Skov et al., 2020), but terrestrial geoscience studies in the area are limited. The first topographic and geomorphic mapping of the area was conducted in 1988 (Pedersen, 1994). The first marine sediment cores from the surrounding fjord system were collected in 2006 (Nørgaard-Pedersen et al., 2008), and a subsequent oceanographic and marine geology campaign provided a history of Atlantic water influx to the fjord system since the last glacial period (Van Nieuwenhove et al., 2020). Research in the area has increased since VRS opened, greatly improving access and logistics for field campaigns. Strunk et al. (2018) established the minimum marine limit and Holocene sea level history of Finderup Land, adjacent to the Prinsesse Ingeborg Halvø in the west, based on cores from five isolation lakes. Additional work on lake sediments and radiocarbon dating of moraine material has elucidated the ice-marginal fluctuations of local ice caps (Larsen et al., 2019), and Larsen et al. (2020) presented the overall deglaciation history of eastern North Greenland.

In this study, we present the ground temperature time series (2014–2021) and sedimentary stratigraphy of two 20-m deep boreholes (SN1 and SN2) at VRS, providing the northernmost analysis of ground thermal regime in Greenland, and the second northernmost worldwide. We aim to (a) provide foundational knowledge of permafrost conditions in the area; (b) explain permafrost evolution, past landscape development, and the potential for future landscape change based on the presented stratigraphy and its physical properties; and (c) understand and quantify the ground thermal regime and how it compares to other high Arctic permafrost monitoring sites. The core analysis is the first stratigraphic investigation of glacial and periglacial deposits in the region. This study provides critical background knowledge for terrestrial studies in the area, and the continuous ground temperature time series will serve as a key data source for the assessment of climate change in this under-studied region of the high Arctic.

2. Study Area

2.1. Geographical and Geological Setting, Glaciation History, and Climate

The Prinsesse Ingeborg Halvø is approximately 20 km long, low-lying (<200 m a.s.l.) and bounded to the east and south by Flade Isblink, the largest independent ice cap in Greenland with an area of 8,500 km^2 (Kelly & Lowell, 2009; Rinne et al., 2011; Figure 1). The peninsula is located at the convergence of the Independence-Danmark Fjord system and the Wandel Sea. Two marine-terminating outlet glaciers of the Greenland Ice Sheet discharge into the ca. 150 km long Independence-Danmark Fjord system. The Kronprins Christian Land peninsula lies on the west side of the Fram Strait, the only location where deep-water exchange with the Arctic Ocean occurs. Cold and fresh waters from the Arctic Ocean flow southward along the east coast of Greenland while warm and saline Atlantic water flows northward along the west coast of Spitsbergen, Svalbard, creating a large climatic gradient across the Fram Strait. The Northeast Water Polynya forms each May on the continental shelf of northeast Greenland, just south of Kronprins Christian Land. Enhanced evaporation over the polynya leads to increased precipitation on Kronprins Christian Land (Schneider & Budéus, 1997).

The bedrock geology of Kronprins Christian Land consists of Phanerozoic fold belts and basins (Dawes, 2009). The northeastern side of the Prinsesse Ingeborg Halvø is composed of Permian and Carboniferous carbonates and shales (Pedersen & Häkansson, 2001; Svennevig, 2018). The southern part of the peninsula and the islands to the northwest are comprised of interbedded fine-grained sandstones, siltstones, and coal of the Paleogene Thyra Ø Formation (Lyck & Stemmerik, 2000; Svennevig, 2018). The peninsula has a partial cover of Quaternary sediments, with numerous beach ridges on the northern tip of the peninsula, which includes the area immediately surrounding VRS, and scattered occurrences of till and alluvial, fluvial, and lacustrine deposits (Pedersen, 1994).

During the Last Glacial Maximum, the Greenland Ice Sheet covered the area, extending onto the Wandel Sea shelf (Nørgaard-Pedersen et al., 2008). The Prinsesse Ingeborg Halvø coastline deglaciated around 11 cal. ka BP, with relatively rapid ice retreat continuing until the ice sheet became land-based around ~8.2 ka (Larsen et al., 2020). The Greenland Ice Sheet reached its present extent around ~6.7 ka in Kronprins Christian Land, and further retreat inwards of the present extent was limited during the Holocene Thermal Maximum (Larsen et al., 2020). After becoming an independent ice cap during deglaciation, Flade Isblink persisted throughout the entire Holocene, but reached a minimum extent (smaller than today) between ~8.7 and 3.1 cal. ka BP (Larsen et al., 2019). During this period, the outlet glaciers of Flade Isblink that bound the Prinsesse Ingeborg Halvø retreated 1.1–2.9 km inside their present margins (Larsen et al., 2019). Relative sea level history of the Prinsesse Ingeborg Halvø has not been studied, but Finderup Land, adjacent to the peninsula to the west, experienced rapid relative sea level fall from 9.5 ± 0.2 to 8.0 cal. ka BP, when the sea level approximately reached the modern-day coastline (Strunk et al., 2018). The marine limit on Finderup Land is at least 81.2 m a.s.l (Strunk et al., 2018).

Between 2002 and 2009, mean surface elevation change and the annual mass change rate of Flade Isblink were near zero (Rinne et al., 2011). This is in contrast to decidedly negative mass balance trends for other Greenland glaciers and ice caps (Bolch et al., 2013) and the Greenland Ice Sheet, which has experienced a sixfold increase in mass loss since the 1980s (Mouginot et al., 2019). Flade Isblink has been losing elevation below the snow line, but this has been countered by elevation gains above the snow line (Rinne et al., 2011), implying that precipitation is key to the ice cap's stability.

Mean annual air temperature (MAAT) at Station Nord was −15.8°C during the 1981–2010 climate normal period and −15.1°C during the 1991–2020 climate normal period, based on the NASA GISS Surface Temperature Analysis (GISTEMP v4) data set (GISTEMP Team, 2021; Lenssen et al., 2019). During the 2014–2021 ground temperature data period, mean annual air temperature at Station Nord ranged from −13.0°C to −15.0°C (Danmarks Meteorologiske Institut, 2021). Average annual precipitation during 2014–2021 was 323 mm (Danmarks Meteorologiske Institut, 2021). The annual precipitation values are comparable to those of the west coast of Spitsbergen, Svalbard, on the other side of the Fram Strait. The average monthly air temperature at Station Nord only exceeds 0°C during the summer months of June, July and August (Danmarks Meteorologiske Institut, 2021). The confluence of the Independence-Danmark Fjord system is covered by semipermanent sea ice, and typically there is only open water immediately surrounding the Prinsesse Ingeborg Halvø from the end of July to early September (Limoges et al., 2018; Figure 1). Sea ice extent was reduced during the Holocene Thermal Maximum and the southern limit of permanent sea ice was around 83°N (Funder et al., 2011), just north of Kronprins Christian Land.

2.2. Study Sites

The two permafrost monitoring boreholes are located ca. 100 m west of the VRS atmospheric observatory (sometimes called monitoring house in other literature). Both boreholes are in raised beach deposits, but SN1 is located slightly higher in elevation (36 m a.s.l.) on flat ground, while SN2 (27 m a.s.l.) is located downslope and approximately 70 m west of SN1. The sites were chosen to capture the effects of local variation in snow thickness. Almost no snow depth measurements are available from directly at the boreholes due to infrequent site visits, specifically in winter. Snow depth probing at the boreholes was carried out twice in 2015: there was 26 cm more snow at SN2 compared to SN1 on 2 February (163 vs. 137 cm), and 47 cm more snow at SN2 compared to SN1 on 17 May (138 vs. 91 cm). Vegetation and soil fauna on the peninsula is limited, with a survey of 10 plots south of Station Nord indicating a vegetation cover of less than 20% percent (Krogh et al., 2020).

3. Methods

3.1. Core Collection, Description, and Laboratory Analysis

A hydraulic-powered, transportable drill rig owned by UNIS was used with 1-m long and 42-mm diameter core barrels (Christiansen et al., 2021) to obtain core samples during the borehole drilling in August 2014. Approximately 6 m of core and 5 m of unconsolidated samples were obtained from SN1, and 5 m of core and 12 m of unconsolidated samples were obtained from SN2. Some strata disintegrated during drilling or were too rocky to be cut through with the coring drill bits, precluding complete core recovery of the full 20 m borehole lengths. The distribution of the core samples over the borehole lengths (Figure 2) and the relatively simple stratigraphy allowed for cryostratigraphic characterization of the sites. The frozen cores were transported to UNIS, where they were split lengthwise, photographed, and described in a laboratory cooled to approximately −8°C. The cores were described sample-by-sample with focus on lithostratigraphy and cryostratigraphy. These photographs and descriptions were used to make the core logs and delineate stratigraphic units based on texture and sedimentary structures.

Subsamples of the cores were taken for the analyses described below. Gravimetric moisture content was determined for 36 and 44 samples of the SN1 and SN2 cores, respectively. Freezing point depression (FPD) and salinity were calculated for 24 samples, 12 from each site. Samples were chosen both to represent observed stratigraphic variations and to provide an even downcore distribution.

Gravimetric moisture content (G_m) is the ratio of the sample's water mass and dry sample mass:

$$G_m = \frac{M_f - M_d}{M_d};\ G_{m,\ \%} = G_m \times 100$$

where M_f is the mass of the frozen sample and M_d is the mass after oven drying (Murton, 2013). Samples for gravimetric moisture content were dried for 24 hours at 90°C.

FPD is the phenomenon where the presence of solutes lowers the freezing temperature of the solvent. Soils commonly contain dissolved salts, but usually at low concentrations, resulting in minimal FPD (French, 2007). However, saline Arctic permafrost can exhibit FPD of multiple degrees, meaning the permafrost contains significant unfrozen water content below 0°C (Gilbert et al., 2019; Wu et al., 2017). Sample freezing points, and thus FPD, were determined by identifying the plateau in the freezing curve of the samples; this plateau occurs because of the latent heat of fusion. Freezing curves were obtained in April 2020 by wrapping selected core samples (ca. 200 g) in aluminum foil and inserting a temperature probe into the middle of each sample. The samples with inserted temperature probes were warmed to at least 4°C, and then were placed in a freezer and cooled to at least −8°C (approximately 1–2.5 hours).

Salinity was determined by soaking ca. 40–100 g of the sample (taken from the FPD samples) in a known mass of deionized water (ca. 500 g/500 mL). The samples were left out at room temperature for at least 1 hour, with occasional stirring, to ensure the samples were thawed and salts were dissolved. Salinity of the mixture, S_m, was measured in parts per thousand (ppt) with a hand-held conductivity meter that was calibrated with standard solutions. Pore water salinity was calculated using known sample masses and calculated gravimetric moisture content:

$$Pore\ water\ salinity,\ ppt = \frac{S_m \times (M_1 + 500)}{M_1};\ M_1 = \frac{G_m \times M_f}{1 + G_m}$$

3.2. Meteorological Data

Air temperature, wind speed and wind direction measured at 9 m height, as well as snow depth data, are automatically measured at the meteorology station next to the VRS atmospheric observatory, less than 100 m from SN1. The measurement interval switched from every half hour to every 5 minutes on 24 April 2017. These data are available through the VRS website (https://villumresearchstation.dk/data/) and are collected by Asiaq, the Greenland Survey. The meteorological time series starts on 26 August 2014 and has occasional multiday data gaps. Air temperature is not measured at 1.5 or 2 m (which is more common) because maximum snow depth can approach these heights. The snow depth time series was cleaned by removing outliers and removing 0 m snow

depth values during the snow season, thus removing some of the large amplitude, instantaneous fluctuations, which can be caused by a variety of factors including a low density snow surface, intense snowfall or snowdrift, high winds, and a disturbed snow surface (i.e., from snow drifting, animal tracks, snow falling off the sensor mounting structure) (Brazenec, 2005). Thawing degree days (TDD; units: °C days) were calculated by summing positive daily mean air temperatures during each hydrological year, and freezing degree days (FDD; units: °C days) were calculated by summing negative daily mean air temperatures during each hydrological year. We use the defined hydrological year of 1 September to 31 August; this period was chosen because the local maxima of the summation curve of daily air temperatures (representing the shift from positive to negative air temperatures) occurred at the end of August for the 2015–2020 summers.

3.3. Ground Temperature Data

Both boreholes were cased with steel pipe and are instrumented with GeoPrecision thermistor strings with DALLAS DS18S20 temperature sensors and integrated M-Log5W data loggers. Temperatures are recorded every six hours (0:00, 06:00, 12:00, 18:00 UTC) at 20 depths: 0 m, 0.05 m, 0.1 m, 0.25 m, 0.5 m, 0.75 m, 1.0 m, 1.5 m, 2.0 m, 2.5 m, 3.0 m, 4.0 m, 6.0 m, 8.0 m, 10.0 m, 12.0 m, 14.0 m, 16.0 m, 18.0 m, and 20.0 m. The thermistor strings have a manufacturer-reported resolution of 0.065°C and accuracy of ±0.25°C at 0°C. The continuous time series presented here span over seven years from 13 August (SN1) and 24 August (SN2) 2014 to 15 December 2021 and are available through the Global Terrestrial Network for Permafrost (GTN-P) database (http://gtnpdatabase.org/). We often refer to the seven-year study period, meaning the seven full hydrological years of ground temperature data from 1 September 2014 to 31 August 2021.

Hydrological year freezing n-factors (n_f) were calculated for SN1 and SN2 using air temperature FDD and surface temperature FDD:

$$n_f = \frac{FDD_s}{FDD_a}$$

where FDD_s is the FDD at the ground surface (0 m) and FDD_a is the air temperature FDD (Klene et al., 2001). Daily mean temperature at 0 m was calculated from the six-hour interval ground temperature data and was used to calculate FDD_s.

ALT was thermally defined and linearly extrapolated using the depth and temperature data from the first two thermistors at or above the zero-degree isotherm. These two points were used to determine the temperature gradient and define a line, and the depth of the zero-degree isotherm was determined by the depth-intercept of this line. Riseborough (2008) found this method of extrapolation to be consistently more accurate than interpolation using data points above and below the zero-degree isotherm. The latest occurring maximum temperature of the thermistor at or above the zero-degree isotherm determined the timestamp of the data points for extrapolation and thus the date of maximum thaw depth. Thermally determined ALT can differ from ALT based on the phase of water (frozen/unfrozen), especially in saline permafrost (Burn, 1998), but we consider this effect to be negligible for the sites based on the uppermost salinity and FDP data, low moisture content overall, and the tendency for pore water solutes to be expulsed downwards from a deepening freezing front during subaerial permafrost growth (Gilbert et al., 2019).

4. Results

4.1. Borehole Stratigraphy

Three stratigraphic units were identified from the collected cores and borehole material (Figure 2). Each unit description is paired with a genetic interpretation; these genetic interpretations are contextualized within the region's landscape development in the discussion. Unfortunately, no datable organic material was found in the cores, as is often the case in Arctic environments with low organic productivity (Strunk et al., 2020) and high-energy depositional environments (e.g., beaches and glacier-adjacent settings).

4.1.1. Unit 1 — Glacial Deposits

This unit was only found within the boreholes in the lowermost portion of SN2, where it is ca. 2 m thick and overlies bedrock, which was encountered around 19.6 m depth. The unit consists of a massive, matrix-supported

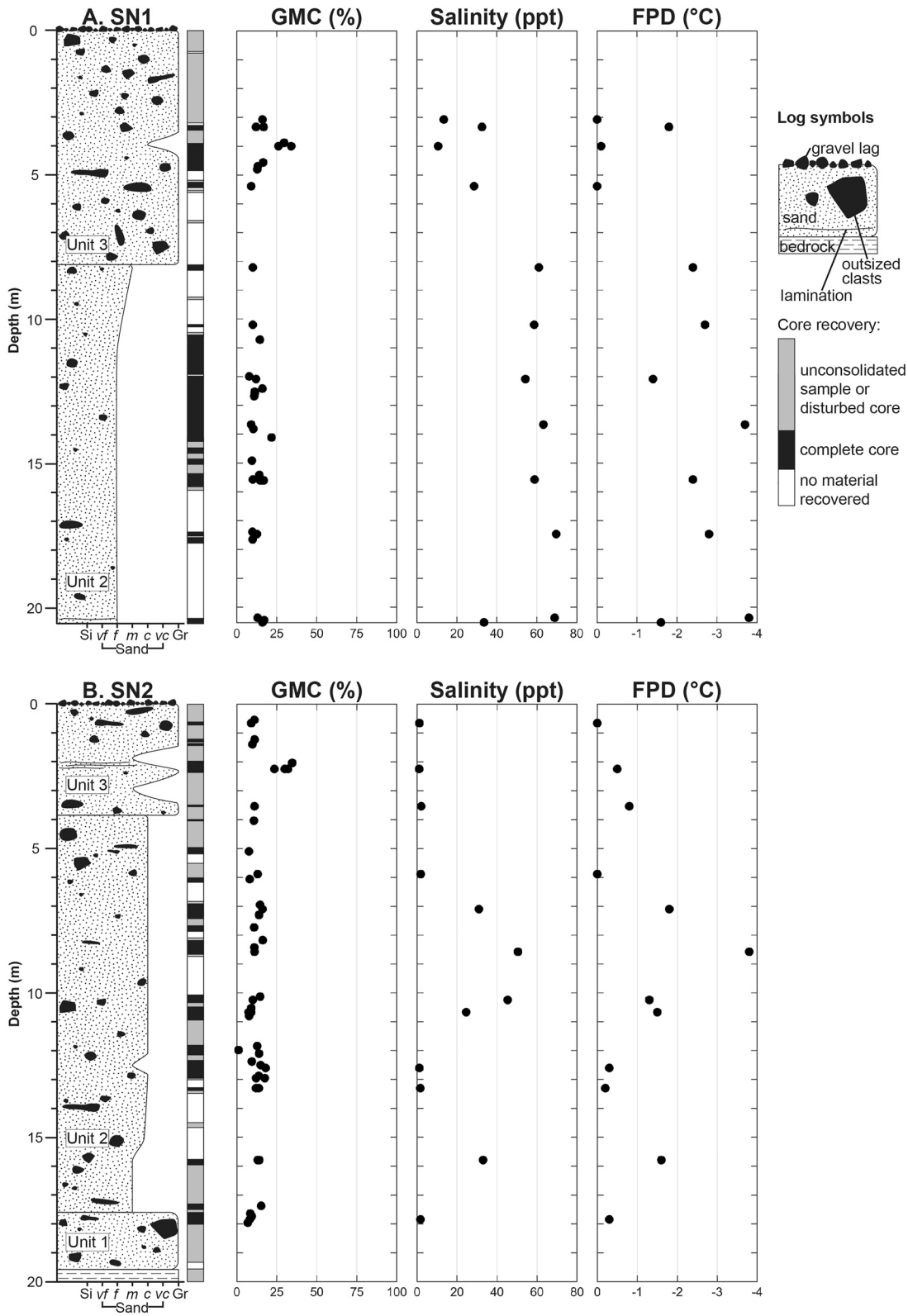

Figure 2. Sedimentological log of the boreholes SN1 (A, top) and SN2 (B, bottom) with corresponding plots of core recovery/core quality, gravimetric moisture content, salinity, and freezing point depression.

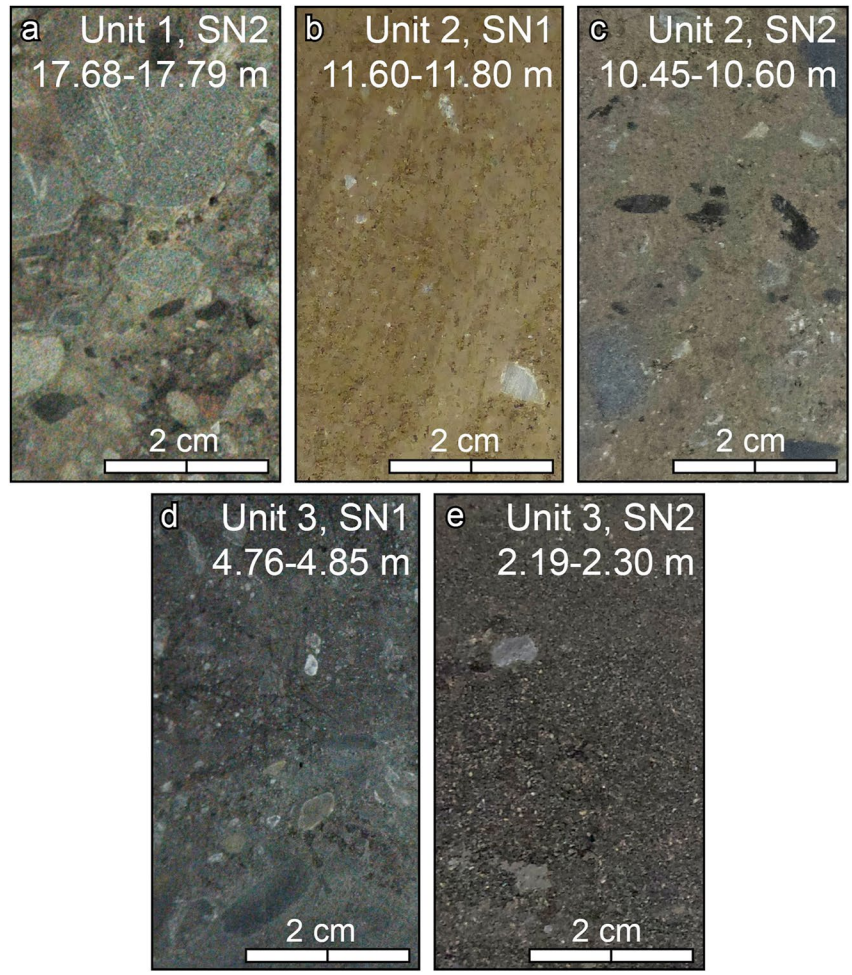

Figure 3. Representative split-core images showing sections of each unit from each core. Each image is labeled with the unit, borehole, and depth interval of the entire core that the photographed section comes from.

diamicton (Figure 3a). The diamicton has a sandy matrix with angular and rounded clasts of gravel size. Given the area's glacial history, this diamicton unit is interpreted as a melt-out or lodgment till formed by glacial advance and retreat over the Prinsesse Ingeborg Halvø.

4.1.2. Unit 2 — Glaciomarine Deposits

Both SN1 and SN2 are predominately comprised of nongraded, massive sand with clasts (Figures 3b and 3c). This unit underlies Unit 3 and is ca. 12 m thick in SN1 and 13 m thick in SN2. The sand in this unit ranges from coarse to fine and is better sorted than in most of Unit 3. Clasts are common, but not as abundant as in Unit 3. Based on the uniform sand matrix with fluctuating clast abundance, this unit is interpreted as a glaciomarine deposit from a shallow marine environment dominated by ice-rafted debris.

4.1.3. Unit 3 — Beach Deposits

The uppermost portion of both SN1 and SN2 is comprised of medium to very coarse sand with clasts of gravel size (Unit 3, ca. 8 m thick at SN1 and 4 m thick at SN2; Figures 3d and 3e). Most samples from this unit have a poorly sorted sandy matrix with abundant clasts. Short intervals of sand with few to no clasts were also observed, as well as one section with normally graded sand and lamination (ca. 2 m at SN2). Based on the varying features of the sand and abundant gravel clasts, this unit is interpreted as a beach deposit from a wave and storm-affected shoreline.

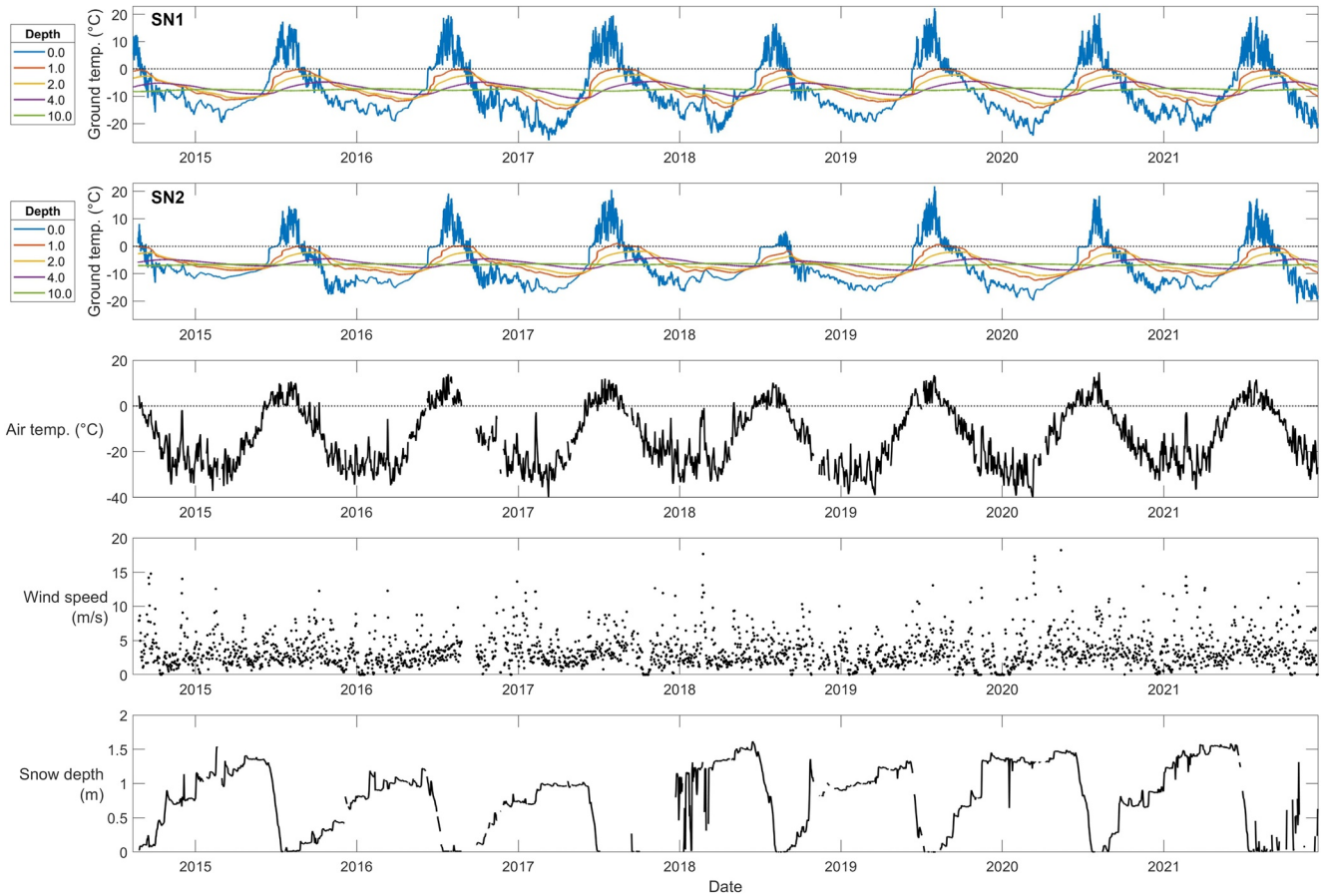

Figure 4. SN1 and SN2 ground temperature time series (August 2014 – December 2021), plotted with air temperature, wind speed, and snow depth during the same time period. The meteorological data shown here are daily values and were measured at the Villum Research Station meteorology station.

4.2. Cryostratigraphy and Physical Properties

Visual inspection revealed that none of the cores contained visible excess ice. The only ice type present was sediment pore-filling ice, where ice is limited to the spaces between sediment grains. This ice type is formed by the freezing of pore water. The absence of visible ice was corroborated by the consistently low moisture content: 90% of the samples (72 of 80) had a gravimetric moisture content less than 20%. Slightly higher moisture content (20%–35%) occurred in a few samples in sandier intervals of the gravelly beach deposits (Unit 3), around 4 m depth at SN1 and 2 m depth at SN2. Given that the cores are comprised of sand and gravel rather than silt, the material is non-frost susceptible and thus does not support the formation of ice lenses, resulting in a homogeneous cryostratigraphy.

Salinity of the samples ranged from 1 to 70 ppt. Unit 3 (beach deposits) had lower salinity than Unit 2 (glacio-marine deposits). At SN2, the salinity of Unit 3 did not exceed 2 ppt, while it ranged from 11 to 33 ppt at SN1. Unit 2 had consistently high salinity at SN1 (34–70 ppt, average of 59 ppt), and greater variability at SN2 (1–50 ppt). Salinity was only measured for one sample in Unit 1 (glacial deposits, only present at SN2) and was 2 ppt.

Greater freezing point depression (FPD) occurs in more saline soils. FPD was between 0°C and −1°C in the lowest salinity samples (<20 ppt). In the more saline Unit 2, FPD was commonly between −1 and −4°C.

4.3. Meteorology

The Station Nord area has long, cold winters. Air temperatures above 0°C typically only occur in June, July, and August (Figure 4). Winter air temperatures (DJF) are the most variable of the four seasons. Spikes in winter air temperature (rapid increase in air temperature followed by rapid decrease, spanning multiple days) do occur in

Table 1
Key Meteorology and Ground Temperature Parameters by Hydrological Year (1 September 2014–31 August 2021)

Parameter	2014/15	2015/16	2016/17	2017/18	2018/19	2019/20	2020/21
MAAT (°C)	−13.8	−14.3	−14.2	−13.2	−14.0	−13.2	−13.2
Min. air temp. (°C)	−37.1	−34.6	−39.9	−34.0	−38.9	−39.9	−36.5
Max. air temp. (°C)	10.6	13.9	12.0	10.2	13.5	14.7	11.5
FDD (°C days)	−5,157	−5,283	−4,816	−4,868	−4,853	−4,921	−4,989
TDD (°C days)	301	324	330	235	335	303	269
Missing air temp. data (days)	14	19	49	15	43	17	7
Max. snow depth (m)	1.54	1.22	1.03	1.62	1.36	1.49	1.58
ALT, SN1 (m)	0.86	0.85	1.03	0.78	1.00	0.86	0.83
ALT, SN2 (m)	0.92	1.03	1.16	0.50	1.14	0.89	0.89
MAGST, SN1 (°C)	−7.7	−7.8	−9.4	−8.4	−8.3	−8.5	−8.9
MAGST, SN2 (°C)	−6.3	−7.7	−7.8	−8.0	−7.7	−8.6	−7.7
MAGT at 1 m, SN1 (°C)	−6.7	−6.6	−7.4	−7.1	−6.8	−7.1	−7.4
MAGT at 1 m, SN2 (°C)	−5.6	−6.2	−6.2	−6.2	−7.2	−6.9	−6.4
MAGT at 20 m, SN1 (°C)	−8.1	−8.0	−7.9	−7.9	−7.8	−7.7	−7.7
MAGT at 20 m, SN2 (°C)	−7.3	−7.2	−7.1	−7.0	−6.9	−7.0	−7.0
n_f, SN1	0.63	0.63	0.83	0.71	0.73	0.72	0.74
n_f, SN2	0.50	0.60	0.69	0.61	0.66	0.70	0.64

Note. MAAT stands for mean annual air temperature, FDD stands for freezing degree days, TDD stands for thawing degree days, ALT stands for active layer thickness, MAGST stands for mean annual ground surface temperature, MAGT stands for mean annual ground temperature, and n_f stands for n-factor.

the winter months but never exceed 0°C. Over the entire 26 August 2014 to 15 December 2021 ground temperature data period, the minimum daily air temperature was −39.9°C (10 March 2017) and the maximum daily air temperature was 14.7°C (7 August 2020). From 2014 to 2021, the mean hydrological year air temperature had a relatively narrow range from −14.3°C to −13.2°C (Table 1). Average TDD of the seven hydrological years was 300°C days (standard deviation = 36°C days), and average FDD was −4,984°C days (standard deviation = 174°C days).

Snow begins to accumulate at the end of August or beginning of September. During most winters, snow depth increased throughout December, January, and February and then remained stable near maximum snow depth during March, April, and May (Figure 4). Snow accumulated earlier in the latter half of the study: snow depth exceeded 1 m in December 2017, 2018, and 2019, and snow depth rapidly increased from 0.48 m to 1.36 m in October 2018. Snow melt and snow depth decrease does not begin until June. Maximum snow depth for the entire study period (and for the 2017/18 hydrological year) was 1.62 m on 15 June 2018. Summer 2018 was the coolest, represented by the lowest TDD value of 235°C days. The combination of deep snow and relatively low summer air temperatures meant the 2018 snowpack was not fully melted until mid-August, approximately one month later than the other years. SN2 was snow free for just a few weeks in August 2018.

The average wind speed during the seven hydrological years of this study was 3.4 m/s. Station Nord has a prominent southwesterly wind direction with most wind speeds less than 10 m/s (96.1% of wind observations; Figure 5). The lowest air temperatures (<−30°C) typically occur with wind speeds less than 10 m/s. Wind speeds over 20 m/s are rare (0.1% of wind observations) and are exclusively south or southeasterly in direction. Wind speeds up to 20 m/s were measured in all directions.

4.4. Ground Thermal Regime

The SN1 and SN2 ground temperature time series (Figure 4) have multiple important differences: (a) permafrost temperature is higher overall at SN2; (b) ground surface temperature has less variability at SN2 compared to SN1; and (c) the amplitude of the annual temperature cycle is smaller at all depths at SN2. The magnitude of

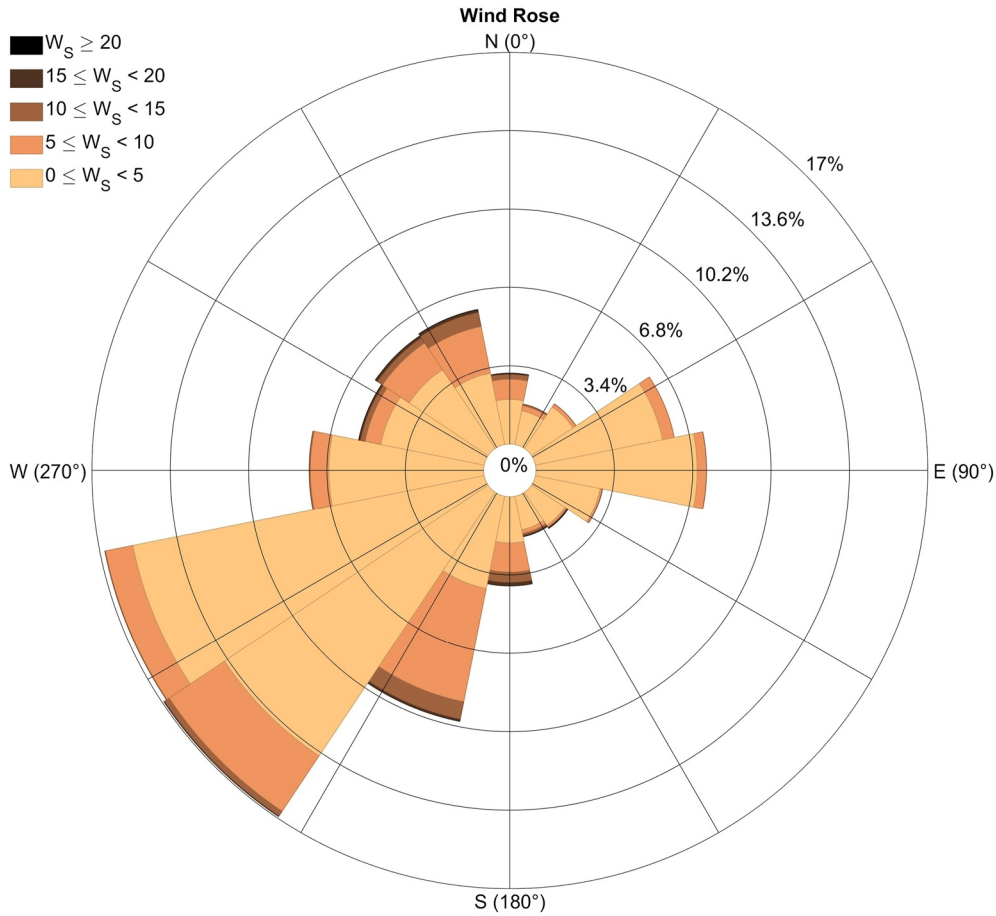

Figure 5. Wind rose for the Villum Research Station meteorology station during the seven hydrological years of this study (1 September 2014–31 August 2021). The units of wind speed (W_s) are m/s.

temperature difference between SN1 and SN2 depends on depth. The difference is greatest in the active layer and close to the ground surface, where temperatures at SN1 are up to 9°C lower than at SN2. At 5 m depth, the winter and average hydrological year temperature profiles (Figure 6) are 1–2°C warmer at SN2. At 20 m, the deepest temperature measurement, the permafrost is 0.8°C warmer at SN2 compared to SN1 (Figure 7). Both sites generally show greater temperature profile variability in winter than in summer, except for the exceptional summer of 2018 at SN2. There is less difference between the seasonal and average temperature profiles at SN2, and thus this site has a narrower ground temperature envelope overall (Figure 6). Ground temperature below 10 m decreases slightly with depth at SN2 and is nearly constant at SN1.

The average 20 m permafrost temperature over the seven-year study period (1 September 2014–31 August 2021) was −7.87°C at SN1 and −7.06°C at SN2. The warming rate at 20 m depth over the study period, assessed by linear regression, was 0.07°C per year at SN1 and 0.05°C per year at SN2 (Figure 7). Average annual temperature variation (hydrological year) at 20 m depth was 0.11°C at SN1 and 0.23°C at SN2, indicating 20 m is slightly shallower than the depth of zero annual amplitude (DZAA) at both boreholes. The average temperature at 1 m depth, the thermistor depth nearest the top of permafrost, was −7.01°C at SN1 and −6.39°C at SN2. Ground surface temperature averaged −8.43°C at SN1 and −7.68°C at SN2, and average n_f was 0.71 at SN1 and 0.63 at SN2 (standard deviation in $n_f = 0.07$ at both sites).

Similar to air temperature, ground surface temperature is typically only above 0°C in the summer months of June, July, and August (Figure 4). Positive near-surface temperatures (which occur down to 1 m at both sites) can occur at the beginning of September. Minimum ground surface temperature at SN1 was −26.06°C (11 March 2017) and −20.87°C at SN2 (29 October 2021). Summer ground surface temperature is relatively similar at SN1 compared to SN2, except for in summer 2018, when the maximum surface temperature was 11.25°C warmer at

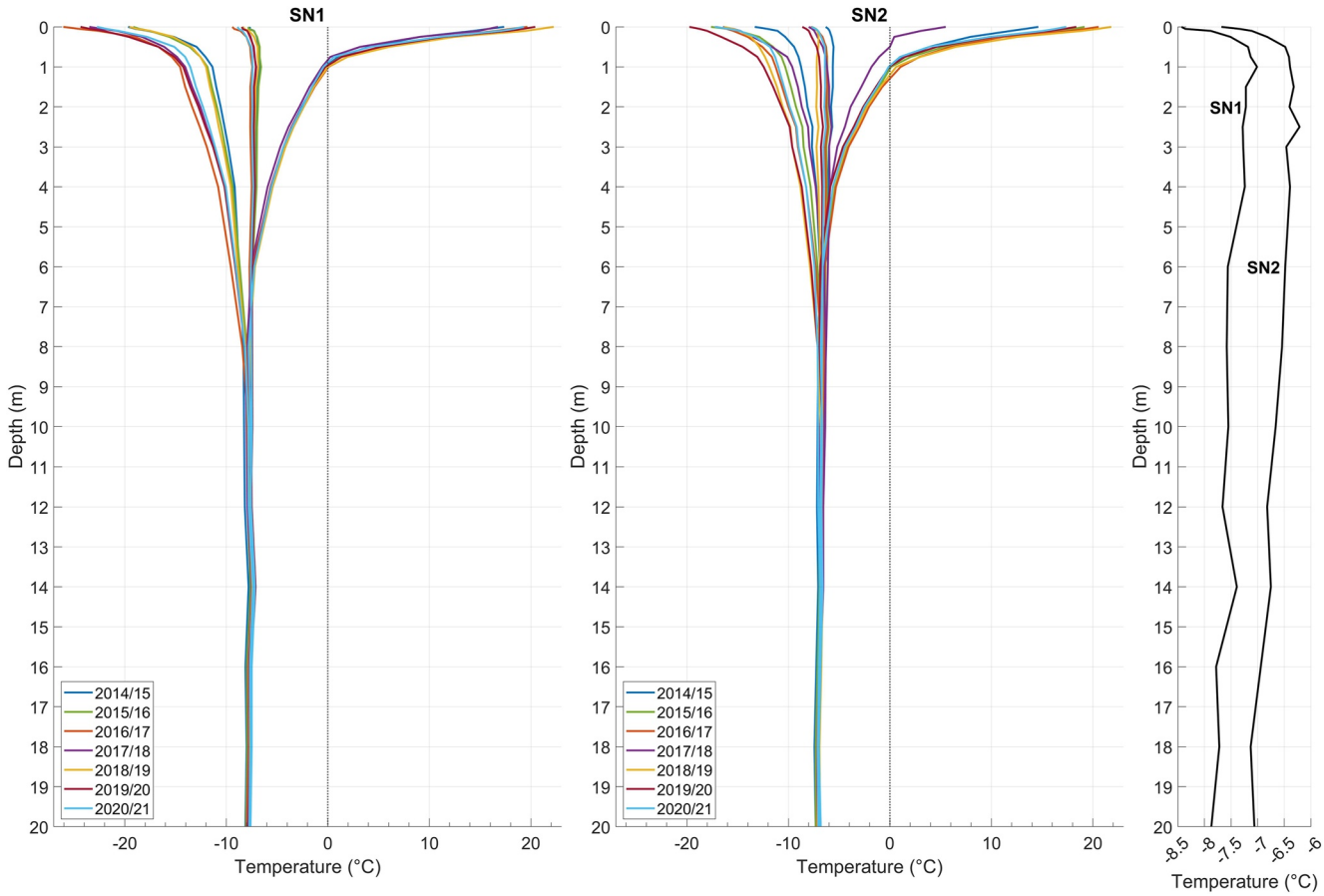

Figure 6. SN1 and SN2 ground temperature envelopes, showing winter minimum, mean, and summer maximum ground temperature profiles for each hydrological year. The rightmost panel shows the overall mean ground temperature profiles for SN1 and SN2, which are the average of the seven hydrological year mean profiles for each site.

SN1 (16.75°C at SN1 compared to 5.5°C at SN2). During this summer, the ground surface temperature at SN2 only became positive at the beginning of August, and temperature at 0.25 cm depth was only positive for approximately 1.5 weeks. This was the coldest summer and the one with the thickest and longest-lasting snow cover, as described in the meteorology section. At SN2, ground surface temperature exhibits the zero-curtain effect, plateauing around 0°C during the snowmelt period before increasing for the remainder of the summer. This only occurs some summers (2016 and 2018) for a short period at SN1. The air temperature signal is reflected in the ground temperature time series at greater depths at SN1; the amplitude of these temperature fluctuations is also larger at SN1 compared to SN2. The amplitude of the annual temperature cycle at 1 m depth is 2°C greater at SN1 compared to SN2 (average hydrological year amplitude of 12.9°C compared to 11.0°C).

Average ALT during the seven-year study period was 0.89 m (standard deviation = 0.09 m) at SN1 and 0.93 m at SN2 (standard deviation = 0.21 m). Active layer thickness was greater at SN2 all years except in 2018, the summer with long-lasting snow, when ALT at SN2 was 0.50 m compared to 0.78 m at SN1 (Figure 7). Maximum thaw depth was typically reached in the second half of August.

5. Discussion

5.1. Landscape Development and Permafrost Evolution on the Prinsesse Ingeborg Halvø

The presented stratigraphy and distribution of ground ice supports the hypothesis that permafrost grew epigenetically in deposits following a deglaciation and isostatic emergence sequence. The Unit 1 diamicton, only present at SN2, is interpreted as till, presumably from when the Prinsesse Ingeborg Halvø was glaciated before 11 cal.

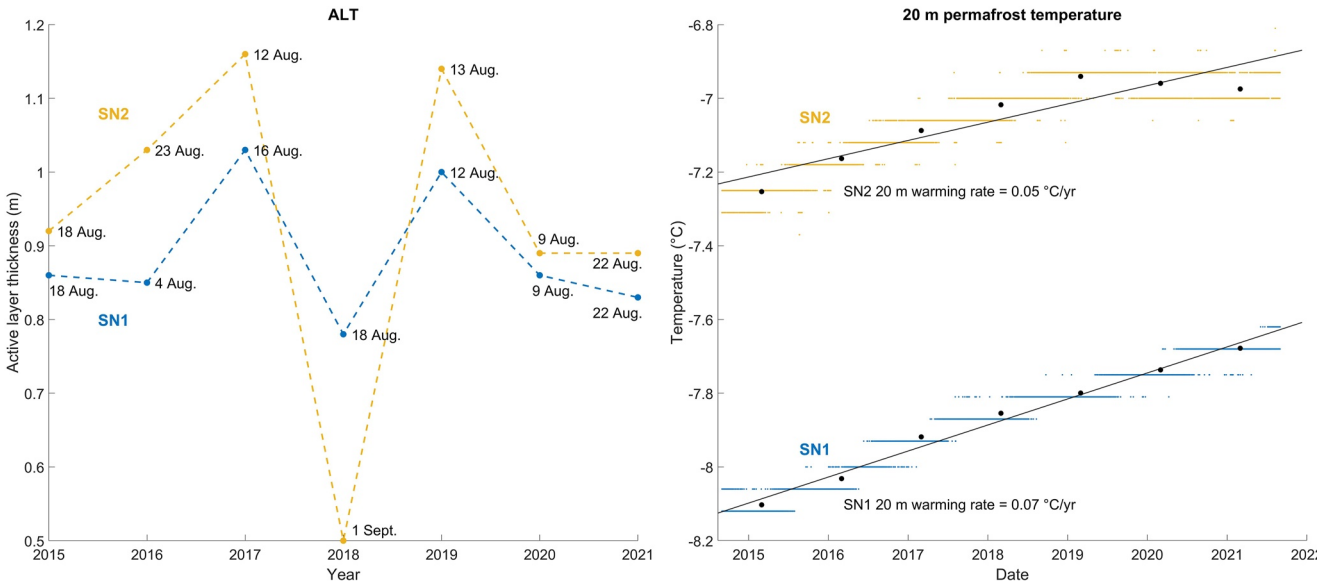

Figure 7. Left: Linearly extrapolated active layer thickness (ALT) at SN1 and SN2; datapoint dates indicate the date of maximum extrapolated thaw depth and thus ALT. Right: Six-hourly 20 m temperature at SN1 and SN2 during the seven-year study period with linear trend lines (in black). The stepped appearance of the data is caused by the 0.065°C resolution of the thermistors. Black dots indicate hydrological year mean temperature at 20 m and are plotted in the middle of the hydrological year which they represent (e.g., 2 March 2015 for the hydrological year 1 September 2014–31 August 2015).

ka BP (Larsen et al., 2020). This till is likely found across the whole peninsula, and thus we expect it would have been found at SN1 had the borehole been drilled to the same depth as SN2, relative to sea level. The details of deposition (i.e., lodgment vs. melt-out) cannot be discerned from the limited core samples available.

During the initial deglaciation of the study area, the fjord surrounding the peninsula would have likely hosted a tidewater glacier, with icebergs and floes depositing ice-rafted debris on the fjord floor. A similar environment exists in outer Danmark Fjord today, but a more expansive calving glacier front was likely present during the early stages of deglaciation. Iceberg production and influx of ice-rafted sediment was likely at a maximum during the most rapid period of ice retreat from 11 to ~8.2 ka (Larsen et al., 2020). Given the location of the boreholes in beach ridges and the marine limit of at least 81 m a.s.l. in neighboring Finderup Land (Strunk et al., 2018), SN1 and SN2 at 36 and 27 m a.s.l., respectively, are clearly below the Prinsesse Ingeborg Halvø marine limit. Thus, glaciomarine Unit 2, which comprises the majority of both boreholes, was deposited in the period between deglaciation and aerial exposure of the sites from relative sea level lowering. The high salinity values of Unit 2 support its marine depositional environment; this is matched by greater freezing point depression in this unit. The salinity values are of the same magnitude as those measured in a fjord-valley system in central Svalbard (Gilbert et al., 2019).

Permafrost aggradation began following emergence. We cannot say when sites SN1 and SN2 were aerially exposed without datable material, but it must have been before 8.0 cal. ka BP, approximately when the present-day coastline was established at Finderup Land (Strunk et al., 2018). Given its higher elevation, SN1 would have been aerially exposed first, and thus has had a slightly longer period for permafrost aggradation and may have slightly thicker permafrost than SN2. A shoreline displacement curve would allow for the determination of site exposure, and is a clear area for future Quaternary research on the Prinsesse Ingeborg Halvø. Unit 3, comprised of beach sands and gravels, formed when the sites were at and near the shoreline. The presence of beach ridges indicates wave action, which means the fjord area surrounding the peninsula must have been sea ice free for at least parts of the year.

This landscape development involved epigenetic permafrost formation, with permafrost forming after the host material was deposited. This is supported by the pore-filling ice observed in the cores, which is indicative of epigenetic permafrost. The sandy substrate does not support the formation of ice lenses and does not contain excess ice. Ground without excess ice warms faster in response to climate change than ground with excess ice, as latent heat is not required for melting ice (Lee et al., 2014). The absence of excess ice also means the land surface

around the sites is relatively resistant to subsidence due to ground ice melting, evidenced by the stable condition of station infrastructure such as the airstrip. However, ice wedge polygons exist in some parts of the peninsula (Humlum et al., 2018), indicating ground ice is present in specific locations. The stratigraphy observed in the cores is less complex compared to permafrost cores taken at Zackenberg, northeast Greenland and near Longyearbyen, Svalbard, locations which have more mountainous terrain and more terrigenous sediment supply resulting in fjord-fill sedimentary successions with delta progradation (Gilbert et al., 2017, 2019).

5.2. The Impact of Snow Dynamics on the Ground Thermal Regime

Snow is a clear driver of the ground thermal regime on the Prinsesse Ingeborg Halvø, and makes the permafrost temperatures relatively high for the extreme high Arctic location and polar tundra climate. Active layer thawing is limited to the short snow-free period, which can be up to 2 months or just a few weeks. The tundra snow cover class is described as having a maximum depth of 75 cm (Sturm et al., 1995), so the snow depths measured at VRS are highly unusual for Arctic tundra environments. Some other Arctic permafrost monitoring sites (i.e., Zackenberg in Greenland and Vorkuta in Russia) have had maximum snow depths that exceed 1 m (Romanovsky et al., 2010; Stiegler et al., 2016), but not on an annual basis like at VRS.

Since SN1 and SN2 have similar stratigraphy, the differences in the ground thermal regime can definitively be attributed to differences in snow cover. Snow is the primary control on the differences in the winter ground temperature profiles in the boreholes, which have larger annual variation than the summer temperature profiles. At SN2, the snow rich site, snow causes an overall dampening of the air temperature signal, its reduced propagation into the ground, and thus a reduced annual temperature cycle amplitude and narrower ground temperature envelope (Figure 6). The greater insulating effect of snow at SN2 compared to SN1 is also evidenced by consistently lower n_f values at SN2. The difference in MAGT temperature between SN1 and SN2 (<2°C) is not even larger because SN1 still has significant snow cover (ca. 1 m), although less than that of SN2.

The timing of initial snow cover and snowpack development affects ground temperatures throughout the hydrological year. Late snow cover and limited autumn snow fall means the ground is more effectively cooled as air temperatures become negative; this was the case in October 2021 when the minimum surface temperature, −20.87°C, was observed at SN2. Minimum surface temperature at SN1 occurred in March 2017 (−26.06°C), when the snow depth was 99 cm. This indicates that autumn and mid-winter air temperatures influence the ground thermal regime while the snowpack develops, even when snow depths are near 1 m. Given the presumed dominance of wind redistributed snow across the Prinsesse Ingeborg Halvø, the snowpack is likely comprised of dense wind slabs and thus has far greater thermal conductivity than freshly fallen snow, allowing for relatively efficient ground cooling in autumn and mid-winter.

Summer 2018 was an outlier, as it had the deepest snow, longest snow duration, and minimum TDD/low summer air temperatures. This phenomenon was not limited to the study area; minimum and near minimum ALT was observed at the Zackenberg Circumpolar Active Layer Monitoring (CALM) sites and is attributed to a large amount of snow and extraordinarily late snow melt (Schmidt et al., 2019; Strand et al., 2021). The Arctic sea ice extent winter maximum was the second smallest on record in 2018 (Scott, 2018), and diminishing Arctic sea ice is linked to anomalously large snowfall in the Northern Hemisphere (Liu et al., 2012). The extraordinary large snowfall in northeast Greenland in 2018 (Schmidt et al., 2019) has not been attributed to specific sea ice conditions, but heavy snowfall in Europe in February 2018 is directly linked to limited sea ice extent and anomalously warm conditions in the Barents Sea (Bailey et al., 2021).

Snowfall and wind redistribution is not just critical for the study area, but to the region in general. The presence of the Northeast Water Polynya leads to increased precipitation on Kronprins Christian Land due to increased evaporation (Schneider & Budéus, 1997). The relatively large amount of snow, especially compared to other polar tundra climates, maintains Flade Isblink's stable mass balance (Bolch et al., 2013; Rinne et al., 2011). The Kronprins Christian Land peninsula is bounded to the west by Danmark Fjord and surrounded to the north and east by ocean that is sea ice-covered most of the year. The dominant southwesterly wind direction at the Prinsesse Ingeborg Halvø may carry wind-drifted snow from across Danmark Fjord to the area. Additionally, winds from the east and northwest may carry snow from the vast sea ice areas. Unfortunately, accurate snow measurements and quantification of snow drift is incredibly difficult, especially in remote locations. The snow regime has undoubtedly changed throughout the area's geologic history, as sea ice extent has changed and in particular was

reduced during the Holocene Thermal Maximum (Funder et al., 2011). Additionally, the Northeast Water Polynya probably did not exist in the early Holocene and at other shorter periods after 5 ka, when there was more open water (Hjort, 1997). Periods in the past with less snow may have contributed to more effective ground cooling and thus increased permafrost aggradation.

Mean precipitation and its interannual variability are projected to increase across the Arctic as a result of climate warming (Bintanja et al., 2020). Increasing Arctic precipitation is mainly attributed to reduced sea ice extent causing increased surface evaporation. Increased snowfall frequency is anticipated in Northern Greenland, including Kronprins Christian Land, in winter (DJF) and spring (MAM) (Lenaerts et al., 2020). Although snowfall is predicted to increase, snow depth on Kronprins Christian Land will not necessarily increase if more wind-transported snow is lost in open water due to decreased sea ice extent. Increasing snow depths typically result in increases in ground temperature in continuous permafrost regions (Park et al., 2015), but this relationship may not hold true for VRS. Should mean snow depth increase at VRS, its effect on the ground temperatures will depend on snowfall timing relative to seasonal air temperature warming as well as snow cover duration. More summers like 2018, when snow cover almost persists through the entire summer, could result in ground cooling.

5.3. Permafrost in Northern Greenland Compared to Surrounding High Arctic Regions

Alert (83°N) on Ellesmere Island is most closely comparable to VRS in terms of climate and latitude, and is the only permafrost monitoring site further north than VRS. Average MAAT at Alert during the 1981–2010 climate normal period was −17.7°C (Environment & Climate Change Canada, 2021), 1.9°C colder than at Station Nord during the same period. MAGT at Alert near the DZAA ranged between −11 and −16°C from 1978 to 2018 at three different boreholes (measurement at either 24 or 15 m; Smith et al., 2019), considerably colder than the −7 to −8°C observed at 20 m depth at SN1 and SN2 from 2014 to 2021. Snow cover is less at the Alert boreholes, with maximum snow depth at the boreholes ranging from <20 to 80 cm (Smith et al., 2012). Average n_f values at the Alert boreholes range from 0.80 to 0.96 (Throop et al., 2012), greater than the average values for SN1 (0.71) and SN2 (0.63), indicating that the winter surface offset, and more specifically the nival (snow) offset, is greater at VRS. The difference in MAGT between VRS and Alert is roughly double the difference in MAAT, also indicating the importance and impact of the thicker snowpack at VRS. Alert and VRS are the only permafrost monitoring sites with a latitude higher than 80°N, and thus the permafrost temperatures at VRS are the warmest observed this far north.

Warming near the DZAA at Alert has occurred since the mid-1990s with a marked increase in the 21st century, following the pattern of Alert's increase in air temperature (Smith et al., 2019). The warming is approximately 0.6°C per decade at 24 m depth and 1.1°C per decade at 15 m from 2000 to 2020 (Smith et al., 2021). In the Arctic continuous permafrost zone overall, permafrost temperature near the DZAA warmed 0.39 ± 0.15°C on average during the decade 2007–2016 (Biskaborn et al., 2019). If we extrapolate the observed 20 m warming rates at VRS of 0.07°C/year and 0.05°C/year from 2014 to 2021, warming is 0.7°C/decade at SN1 and 0.5°C/decade at SN2. We cannot directly compare these extrapolated warming rates to those observed across the Arctic given the variety in time periods used for calculation. However, we can generally say the extrapolated decadal warming rates at VRS are similar to rates reported since 2000 in Svalbard, the Canadian High Arctic, the Alaskan Arctic Coastal Plain, the Northern Mackenzie Valley, and some sites in Siberia (Biskaborn et al., 2019; Romanovsky et al., 2016; Smith et al., 2021).

Smith et al. (2012) attributed ground temperature warming at polar desert sites with minimal snow cover like Alert to increase in autumn and winter air temperatures, which have increased more than spring and summer temperatures. In general, the tundra sites of Ellesmere Island respond more to increasing air temperatures than lower-latitude forested sites where there is a greater surface offset from vegetation and trapped snow (Smith et al., 2019). The largest seasonal air temperature increase has also occurred during winter on Svalbard (Hanssen-Bauer et al., 2019), and winter air temperatures significantly impact ALT at sites with thin winter snow cover (Strand et al., 2021). The average seasonal air temperature record at Station Nord, obtained from the GISTEMP v4 data set (GISTEMP Team, 2021; Lenssen et al., 2019), shows that seasonal air temperature increase is also greatest in winter (DJF) at Station Nord, and second greatest in autumn (SON). This was especially pronounced over the last three decades; from 1990 to 2020 mid-winter (DJF) air temperature increase was 1.6°C per decade, compared to an annual air temperature increase of 0.8°C/decade, assessed by linear regression (Figure 8).

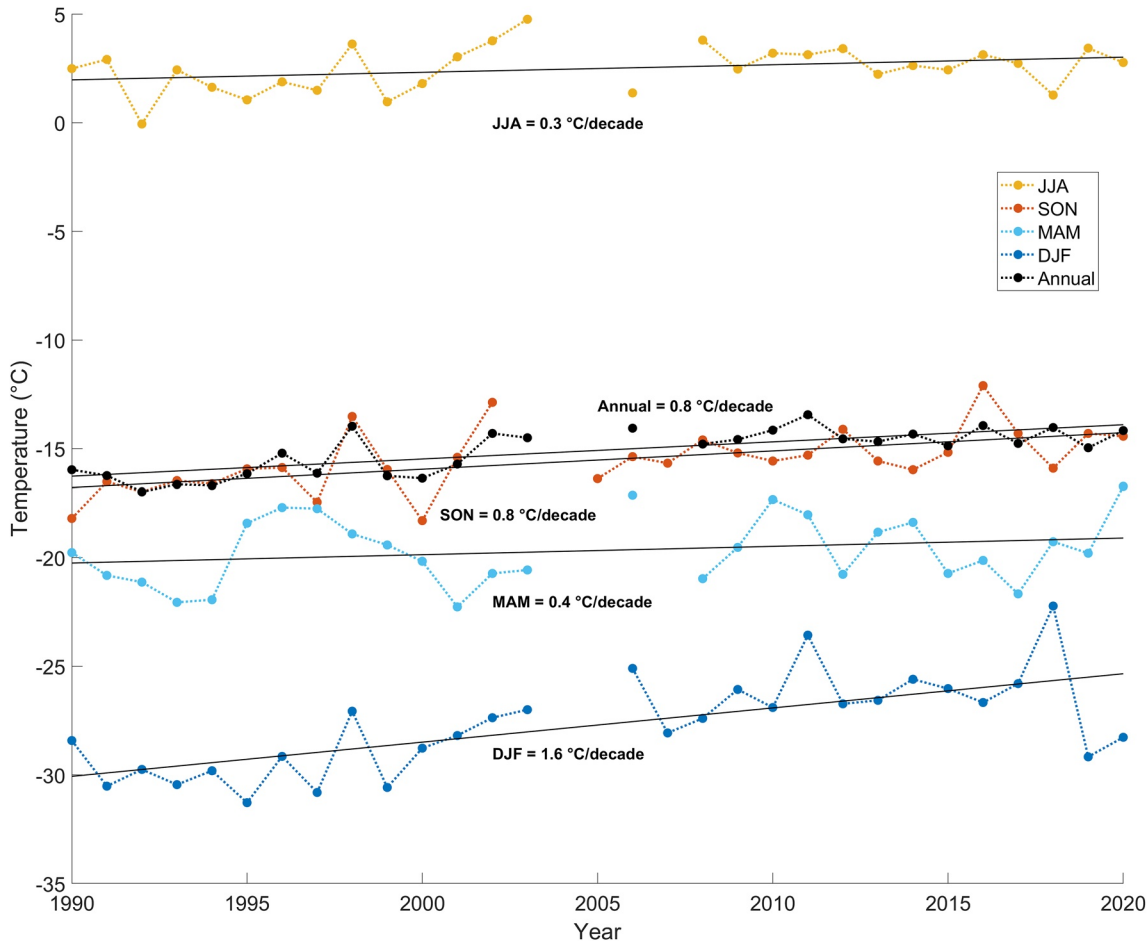

Figure 8. Seasonal and annual air temperature at Station Nord, 1990–2020, obtained from the NASA GISS Surface Temperature Analysis (GISTEMP v4) data set (GISTEMP Team, 2021; Lenssen et al., 2019). The data is adjusted and homogenized (cleaned) station observations. Linear trend lines (black) show seasonal and annual increase, and are labeled with the decadal increase rate. DJF = December-January-February, MAM = March-April-May, JJA = June-July-August, and SON = September-October-November.

Thule and Zackenberg, the other sites in northern Greenland with permafrost boreholes, are both warmer than Station Nord. MAAT is approximately −11°C at Thule (Bjella, 2013) and −9°C at Zackenberg (Hansen et al., 2008; Ploeg et al., 2021). Permafrost temperature at the DZAA (7.6 m) at Thule is −10°C (Bjella, 2013), and 10 m temperatures at Zackenberg are −5.2°C at a snowdrift site and −6.7°C at the meteorological station where there are average snow conditions (Westermann et al., 2015). Based on 10 m, this means permafrost temperatures at VRS are higher than at Thule and slightly lower than at Zackenberg. In central Spitsbergen, Svalbard, temperatures at 10–15 m are considerably higher, ranging from ca. −2°C to −5°C over the 2016–2018 period (Christiansen et al., 2021). These temperatures are clearly related to the far warmer climate on Svalbard; MAAT in Longyearbyen (central Svalbard) averaged −2.2°C from 2016 to 2020 (Norwegian Centre for Climate Services, 2021).

Average ALT at VRS 2015–2018, which was 88 cm at SN1 and 90 cm at SN2, is somewhat greater than at Zackenberg during the same period (when overlapping data is available), where average ALT was 75 and 61 cm at two different CALM sites (Strand et al., 2021). The thinner active layer at Zackenberg is caused by finer-grained sediments, more moisture, and more vegetation compared to VRS. The active layer in the glacial sediments around Thule ranges widely, from 30 cm in vegetated areas to 2 m at unvegetated sites (Bjella, 2015). ALT on Svalbard is generally thicker than at VRS, with most sites having an active layer 1–2 m thick (Christiansen et al., 2021). A permafrost monitoring borehole on the central west coast of Spitsbergen, Kapp Linné 2, was drilled in a raised beach deposit, which overlies bedrock at 6.2 m depth (Christiansen et al., 2010), and thus has comparable upper

stratigraphy to the VRS boreholes. However, ALT at Kapp Linné 2 is nearly 2 m, double that of the VRS boreholes, due to much higher air temperatures and very thin snow cover on the west coast of Svalbard.

ALT at VRS has high variability over the short study period. This is caused by varying snow thickness and timing of snow melt as well as the ice-poor, sandy substrate. The substrate has a relatively high thermal conductivity and energy is not lost to the phase change of ground ice, meaning the short and cool summers still generally lead to the development of an almost 1-m thick active layer. ALT was thinner, 78 cm at SN1 and 50 cm at SN2, when the snow-free period was unusually short in 2018. ALT increase is observed across the Arctic, but high interannual variability in extrapolated ALT at VRS obscures any potential trend in this relatively short data series. Given that summer exhibits the smallest temperature increase at Station Nord (Figure 8), and snow cover is so long-lasting, there might not be an increasing trend in ALT, even across a longer data series. ALT at VRS is highly dependent on the length of the snow-free period, and thus changes in this metric, rather than air temperature, are likely to primarily control future trends in ALT.

6. Conclusions

VRS is located in a complex setting, where fluctuations in glaciation, relative sea level, and sea ice extent have impacted climate, landscape development, permafrost formation, and the present permafrost thermal state. Epigenetic permafrost at this location formed since the Last Glacial Maximum, aggrading as the land became aerially exposed from sea level lowering. The sandy till, glaciomarine, and beach deposits that comprise the upper 20 m of sediments at VRS have low moisture content and no excess ice, making the land surface resistant to subsidence caused by ground warming. However, the relatively high thermal conductivity of the sediments means the ground is reactive to air temperature changes and climate warming.

The Prinsesse Ingeborg Halvø is incredibly unique compared to other polar tundra regions, as the area has thick (>1 m) winter snow cover that almost persists through the entire summer in some locations. This thick and long-lasting snow cover makes the permafrost quite warm for the cold climate and greatly impacts the winter ground thermal regime, and in summers with long-lasting snow cover, active layer development. The permafrost temperatures at VRS are the warmest observed above 80°N. In our seven-year study period, the warming rate at 20 m depth was 0.07°C/year at SN1 and 0.05°C/year at SN2; these rates are similar to those observed since 2000 at other high Arctic sites.

The interplay between snow dynamics, specifically snow timing and depth, and seasonal air temperatures is the most important element controlling the ground thermal regime at this location. Air temperatures during autumn and mid-winter, the fastest warming seasons, clearly influence the ground thermal regime despite a snowpack that exceeds 1 m. This is possible due to the gradual increase in snow depth throughout the snow season and the density of the snowpack arising from the dominance of wind-redistributed snow. We anticipate continued permafrost warming on the Prinsesse Ingeborg Halvø, in line with the area's air temperature increase. Land surface change will be limited due to the absence of excess ice. Increased precipitation is predicted for northeast Greenland and the Arctic overall; the effect of this on snow depth and permafrost conditions on the Prinsesse Ingeborg Halvø will depend on sea ice extent and conditions for wind-redistributed snow, along with the seasonal precipitation distribution and the length of the snow cover period.

Data Availability Statement

All data related to the permafrost boreholes (e.g., ground temperature time series, core and drilling information, laboratory analyses of samples) as well as the meteorological data are openly available through Zenodo via the DOI 10.5281/zenodo.6335754. The ground temperature data are also available in the Global Terrestrial Network for Permafrost database in the boreholes section, accessible at http://gtnpdatabase.org/boreholes. In this database, the boreholes are named Villum Research Station Site 1 and Villum Research Station Site 2. The meteorological data is also accessible at https://www2.dmu.dk/asiaqmet/Default.aspx (the user defines the desired data period); this link is accessible via the VRS website on the data page (https://villumresearchstation.dk/data/). The average seasonal air temperature data for Station Nord, used to discuss climate development, are available through the NASA GISS Surface Temperature Analysis data set as station data, using the station name Station Nord (https://data.giss.nasa.gov/gistemp/station_data_v4/).

Acknowledgments
The authors are grateful for the opportunity to collaborate with Villum Research Station (VRS) on permafrost monitoring as part of their climate monitoring program. When VRS was established in 2014, the permafrost researchers at the University Centre in Svalbard (UNIS) were asked to establish the permafrost monitoring sites as the closest neighboring institution with a permafrost drill rig that could be transported by air to Station Nord. Wesley Farnsworth, Graham Gilbert, and Ullrich Neumann (Kolibri Geo Services) drilled the boreholes and collected the samples in August 2014. We would like to thank Luca Durstewitz for her sample preparation work (core cutting, cataloging, and photographing) and initial lab analysis (gravimetric moisture content and sieving) during her internship at UNIS in spring 2019. Jørgen Skafte and Kirsten Christoffersen kindly assisted with downloading the borehole temperature data in summer 2019 and winter 2021. We would like to thank the Station Nord military personnel and the staff and researchers associated with VRS for helping with logistics and contributing to an excellent fieldwork and research environment. Prof. Henrik Skov has been particularly supportive of this project and ensured successful fieldwork in August 2017. This research received funding from INTERACT under the European Union H2020 Grant Agreement No.871120; this funding covered the summer 2017 fieldwork costs through INTERACT's transnational access program.

References

Bailey, H., Hubbard, A., Klein, E. S., Mustonen, K.-R., Akers, P. D., Marttila, H., & Welker, J. M. (2021). Arctic sea-ice loss fuels extreme European snowfall. *Nature Geoscience*, *14*(5), 283–288.

Bintanja, R., van der Wiel, K., Van der Linden, E., Reusen, J., Bogerd, L., Krikken, F., & Selten, F. (2020). Strong future increases in Arctic precipitation variability linked to poleward moisture transport. *Science Advances*, *6*(7), eaax6869.

Biskaborn, B. K., Smith, S. L., Noetzli, J., Matthes, H., Vieira, G., Streletskiy, D. A., et al. (2019). Permafrost is warming at a global scale. *Nature Communications*, *10*(1), 1–11.

Bjella, K. (2013). *Thule Air Base Airfield White Painting and Permafrost Investigation: Phases I-IV (report no. 13-8)*. U.S. Army Engineer Research and Development Center, Cold Regions Research and Engineering Laboratory. Retrieved from https://usace.contentdm.oclc.org/digital/collection/p266001coll1/id/4363/

Bjella, K. (2015). *Geotechnical Study and Foundation Structural Design, Next Generation Ionosonde (NEXION) Installation, Thule Air Base, Greenland*. Cold Regions Research and Engineering Laboratory. Retrieved from https://apps.dtic.mil/sti/citations/ADA622109

Bolch, T., Sandberg Sørensen, L., Simonsen, S. B., Mölg, N., Machguth, H., Rastner, P., & Paul, F. (2013). Mass loss of Greenland's glaciers and ice caps 2003–2008 revealed from ICESat laser altimetry data. *Geophysical Research Letters*, *40*(5), 875–881.

Brazenec, W. A. (2005). Evaluation of ultrasonic snow depth sensors for automated surface observing systems. (ASOS) [MSc thesis, Colorado State University]. Colorado Climate Center. Retrieved from https://ccc.atmos.colostate.edu/pdfs/Brazenec_Thesis_ALL.pdf

Burn, C. R. (1998). The active layer: Two contrasting definitions. *Permafrost and Periglacial Processes*, *9*(4), 411–416.

Cable, S., Christiansen, H. H., Westergaard-Nielsen, A., Kroon, A., & Elberling, B. (2018). Geomorphological and cryostratigraphical analyses of the Zackenberg Valley, NE Greenland and significance of Holocene alluvial fans. *Geomorphology*, *303*, 504–523.

Christiansen, H. H., Etzelmüller, B., Isaksen, K., Juliussen, H., Farbrot, H., Humlum, O., et al. (2010). The thermal state of permafrost in the nordic area during the international polar year 2007–2009. *Permafrost and Periglacial Processes*, *21*(2), 156–181.

Christiansen, H. H., Gilbert, G., Neumann, U., Demidov, N., Guglielmin, M., Isaksen, K., et al. (2021). Ground ice content, drilling methods and equipment and permafrost dynamics in Svalbard 2016-2019 (PermaSval). In *SESS report 2019-The State of Environmental Science in Svalbard*. https://doi.org/10.5281/zenodo.4294095

Christiansen, H. H., Sigsgaard, C., Humlum, O., Rasch, M., & Hansen, B. U. (2008). Permafrost and periglacial geomorphology at Zackenberg. *Advances in Ecological Research*, *40*, 151–174.

Danmarks Meteorologiske Institut (DMI). (2021). Vejrarkiv [database] https://www.dmi.dk/vejrarkiv/

Dawes, P. R. (2009). The bedrock geology under the inland ice: The next major challenge for Greenland mapping. *Geological Survey of Denmark and Greenland Bulletin*, *17*, 57–60.

Environment, & Climate Change Canada. (2021). *Canadian climate normals, 1981-2010 climate normals & averages*. [database] Retrieved from https://climate.weather.gc.ca/climate_normals/

French, H. M. (2007). *The Periglacial Environment* (3rd ed.): John Wiley & Sons.

Funder, S., Goosse, H., Jepsen, H., Kaas, E., Kjær, K. H., Korsgaard, N. J., et al. (2011). A 10,000-year record of Arctic Ocean sea-ice variability—View from the beach. *Science*, *333*(6043), 747–750.

Gilbert, G., Instanes, A., Sinitsyn, A., & Aalberg, A. (2019). Characterization of two sites for geotechnical testing in permafrost: Longyearbyen, Svalbard. *AIMS Geosciences*, *5*(4), 868–885. https://doi.org/10.3934/geosci.2019.4.868

Gilbert, G. L., Cable, S., Thiel, C., Christiansen, H. H., & Elberling, B. (2017). Cryostratigraphy, sedimentology, and the late Quaternary evolution of the Zackenberg River delta, northeast Greenland. *The Cryosphere*, *11*(3), 1265–1282.

GISTEMP Team. (2021). *GISS surface temperature analysis (GISTEMP)*. NASA Goddard Institute for Space Studies. version 4 [database]. Retrieved from https://data.giss.nasa.gov/gistemp/

Global Climate Observing System. (2021). *Permafrost. Essential climate variables*. Retrieved from https://gcos.wmo.int/en/essential-climate-variables/permafrost/

Global Terrestrial Network for Permafrost (GTN-P). (2021). *Boreholes – permafrost temperatures* [database]. Arctic Portal and the Alfred Wegener Institute. Retrieved from http://gtnpdatabase.org/boreholes

Hansen, B. U., Sigsgaard, C., Rasmussen, L., Cappelen, J., Hinkler, J., Mernild, S. H., et al. (2008). Present-day climate at Zackenberg. *Advances in Ecological Research*, *40*, 111–149.

Hanssen-Bauer, I., Førland, E., Hisdal, H., Mayer, S., Sandø, A., & Sorteberg, A. (2019). *Climate in Svalbard 2100 - a knowledge base for climate adaptation*. (Report no. 1/2019). Norewegian Centre for Climate Services (NCCS). Retrieved from https://www.miljodirektoratet.no/globalassets/publikasjoner/m1242/m1242.pdf

Hjort, C. (1997). Glaciation, climate history, changing marine levels and the evolution of the Northeast Water Polynya. *Journal of Marine Systems*, *10*(1–4), 23–33.

Humlum, O., Farnsworth, W. R., & Strand, S. M. (2018). TRANSGREEN activities at Villum research station in 2017. In *Villum Research Station, Station Nord 2017 Annual report*. Retrieved from https://villumresearchstation.dk/fileadmin/villumresearchstation/AnnualReports/VRS2017_AnnualReport_web3.pdf

IPCC. (2021). In V. Masson-Delmotte, P. Zhai, A. Pirani, S. L. Connors, C. Péan, S. Berger, et al. (Eds.), *Climate Change 2021: The Physical Science Basis. Contribution of Working Group I to the Sixth Assessment Report of the Intergovernmental Panel on Climate Change*. Cambridge University Press. In Press.

Jakobsson, M., Mayer, L., Coakley, B., Dowdeswell, J. A., Forbes, S., Fridman, B., et al. (2012). The international bathymetric chart of the Arctic Ocean (IBCAO) version 3.0. *Geophysical Research Letters*, *39*(12).

Kelly, M. A., & Lowell, T. V. (2009). Fluctuations of local glaciers in Greenland during latest Pleistocene and Holocene time. *Quaternary Science Reviews*, *28*(21–22), 2088–2106.

Klene, A. E., Nelson, F. E., Shiklomanov, N. I., & Hinkel, K. M. (2001). The n-factor in natural landscapes: Variability of air and soil-surface temperatures, Kuparuk River Basin, Alaska, USA. *Arctic Antarctic and Alpine Research*, *33*(2), 140–148.

Krogh, P. H., Gjelstrup, P., Hansen, O. L. P., & Høye, T. T. (2020). Soil fauna of Princess Ingeborg Peninsula. Poster presented at the 3rd Workshop on Field Studies at the Villum Research Station (VRS). Retrieved from https://pure.au.dk/portal/files/177403453/StN_poster_A4.pdf

Larsen, N. K., Levy, L. B., Strunk, A., Søndergaard, A. S., Olsen, J., & Lauridsen, T. L. (2019). Local ice caps in finderup Land, north Greenland, survived the Holocene thermal maximum. *Boreas*, *48*(3), 551–562.

Larsen, N. K., Søndergaard, A. S., Levy, L. B., Olsen, J., Strunk, A., Bjørk, A. A., & Skov, D. (2020). Contrasting modes of deglaciation between fjords and inter-fjord areas in eastern North Greenland. *Boreas*, *49*(4), 903–917.

Lee, H., Swenson, S. C., Slater, A. G., & Lawrence, D. M. (2014). Effects of excess ground ice on projections of permafrost in a warming climate. *Environmental Research Letters*, *9*(12), 124006.

Lenaerts, J., Camron, M. D., Wyburn-Powell, C. R., & Kay, J. E. (2020). Present-day and future Greenland ice sheet precipitation frequency from CloudSat observations and the community Earth system model. *The Cryosphere*, *14*(7), 2253–2265.
Lenssen, N. J., Schmidt, G. A., Hansen, J. E., Menne, M. J., Persin, A., Ruedy, R., & Zyss, D. (2019). Improvements in the GISTEMP uncertainty model. *Journal of Geophysical Research: Atmospheres*, *124*(12), 6307–6326.
Limoges, A., Ribeiro, S., Weckström, K., Heikkilä, M., Zamelczyk, K., Andersen, T. J., et al. (2018). Linking the modern distribution of biogenic proxies in high Arctic Greenland shelf sediments to sea ice, primary production, and Arctic-Atlantic inflow. *Journal of Geophysical Research: Biogeosciences*, *123*(3), 760–786.
Liu, J., Curry, J. A., Wang, H., Song, M., & Horton, R. M. (2012). Impact of declining Arctic sea ice on winter snowfall. *Proceedings of the National Academy of Sciences*, *109*(11), 4074–4079.
Lyck, J. M., & Stemmerik, L. (2000). Palynology and depositional history of the Paleocene? Thyra Ø Formation, Wandel Sea basin, eastern North Greenland. *Geology of Greenland Survey Bulletin*, *187*, 21–49.
Mouginot, J., Rignot, E., Bjørk, A. A., Van Den Broeke, M., Millan, R., Morlighem, M., et al. (2019). Forty-six years of Greenland Ice Sheet mass balance from 1972 to 2018. *Proceedings of the National Academy of Sciences*, *116*(19), 9239–9244.
Murton, J. B. (2013). Ground ice and cryostratigraphy. In R. G. A. J. Harbor (Ed.), *Treatise on Geomorphology: Glacial and Periglacial Geomorphology* (Vol. 8, pp. 173–201). Academic Press.
Nørgaard-Pedersen, N., Mikkelsen, N., & Kristoffersen, Y. (2008). Late glacial and Holocene marine records from the Independence Fjord and Wandel Sea regions, North Greenland. *Polar Research*, *27*(2), 209–221.
Norwegian Centre for Climate Services. (2021). Seklima, Observations and weather statistics [database]. Retrieved from https://seklima.met.no/observations/
Park, H., Fedorov, A. N., Zheleznyak, M. N., Konstantinov, P. Y., & Walsh, J. E. (2015). Effect of snow cover on pan-Arctic permafrost thermal regimes. *Climate Dynamics*, *44*(9), 2873–2895.
Pedersen, S. A. S. (1994). *Geological Map of Prinsesse Ingeborg Halvø, Kronprins Christian Land, North Greenland*. Retrieved from https://data.geus.dk/maparchive/ViewMap.xhtml?mapMapId=4218
Pedersen, S. A. S., & Håkansson, E. (2001). Kronprins Christian land orogeny deformational styles of the end Cretaceous transpressional mobile belt in eastern North Greenland. *Polarforschung*, *69*, 117–130.
Ploeg, K., Seemann, F., Wild, A.-K., & Zhang, Q. (2021). Glacio-nival regime creates complex relationships between discharge and climatic trends of Zackenberg river, Greenland (1996–2019). *Climate*, *9*(4), 59.
Rasmussen, L. H., Zhang, W., Hollesen, J., Cable, S., Christiansen, H. H., Jansson, P.-E., & Elberling, B. (2018). Modelling present and future permafrost thermal regimes in Northeast Greenland. *Cold Regions Science and Technology*, *146*, 199–213.
Rinne, E., Shepherd, A., Palmer, S., Van Den Broeke, M., Muir, A., Ettema, J., & Wingham, D. (2011). On the recent elevation changes at the Flade Isblink Ice Cap, northern Greenland. *Journal of Geophysical Research*, *116*(F3).
Riseborough, D. (2008). *Estimating active layer and talik thickness from temperature data: implications from modeling results*. Paper presented at the Ninth international conference on permafrost. Institute of Northern Engineering, University of Alaska Fairbanks.
Romanovsky, V., Smith, S., Shiklomanov, N., Streletskiy, D., Isaksen, K., Kholodov, A., et al. (2016). Terrestrial permafrost [in "State of the Climate in 2016"]. *Bulletin of the American Meteorological Society*, *98*(8).
Romanovsky, V. E., Drozdov, D., Oberman, N. G., Malkova, G., Kholodov, A. L., Marchenko, S., et al. (2010). Thermal state of permafrost in Russia. *Permafrost and Periglacial Processes*, *21*(2), 136–155.
Schmidt, N. M., Reneerkens, J., Christensen, J. H., Olesen, M., & Roslin, T. (2019). An ecosystem-wide reproductive failure with more snow in the Arctic. *PLoS Biology*, *17*(10), e3000392.
Schneider, W., & Budéus, G. (1997). Summary of the Northeast water polynya formation and development (Greenland sea). *Journal of Marine Systems*, *10*(1–4), 107–122.
Schomacker, A., Larsen, N. K., Bjørk, A. A., & Kjær, K. H. (2017). Temperature observations from northernmost Greenland, 2006-2010. *Low Temperature Science*, *75*, 85–90. https://doi.org/10.14943/lowtemsci.75.85
Scott, M. (2018). Arctic sea ice extent at 2018 winter maximum was second smallest on record. *Arctic Sea Ice News and Analysis*. National Snow and Ice Data Center. Retrieved from https://www.climate.gov/news-features/featured-images/arctic-sea-ice-extent-2018-winter-maximum-was-second-smallest-record
Skov, H., Hjorth, J., Nordstrøm, C., Jensen, B., Christoffersen, C., Bech Poulsen, M., et al. (2020). Variability in gaseous elemental mercury at Villum Research Station, Station Nord, in north Greenland from 1999 to 2017. *Atmospheric Chemistry and Physics*, *20*(21), 13253–13265.
Smith, S., Duchesne, C., & Lewkowicz, A. (2019). Tracking changes in permafrost thermal state in Northern Canada. In *Cold Regions Engineering 2019* (pp. 670–677). American Society of Civil Engineers. https://ascelibrary.org/doi/abs/10.1061/9780784482599.077
Smith, S., Romanovsky, V., Lewkowicz, A., Burn, C. R., Allard, M., Clow, G., et al. (2010). Thermal state of permafrost in North America: A contribution to the international polar year. *Permafrost and Periglacial Processes*, *21*(2), 117–135.
Smith, S., Throop, J., & Lewkowicz, A. G. (2012). Recent changes in climate and permafrost temperatures at forested and polar desert sites in northern Canada. *Canadian Journal of Earth Sciences*, *49*(8), 914–924.
Smith, S. L., Romanovsky, V. E., Isaksen, K., Nyland, K. E., Kholodov, A. L., Shiklomanov, N. I., et al. (2021). Permafrost [in "State of the Climate in 2020"]. *Bulletin of the American Meteorological Society*, *102*(8), S293–S297. https://doi.org/10.1175/BAMS-D-21-0086.1
Stiegler, C., Lund, M., Christensen, T. R., Mastepanov, M., & Lindroth, A. (2016). Two years with extreme and little snowfall: Effects on energy partitioning and surface energy exchange in a high-arctic tundra ecosystem. *The Cryosphere*, *10*(4), 1395–1413.
Strand, S. M., Christiansen, H. H., Johansson, M., Åkerman, J., & Humlum, O. (2021). Active layer thickening and controls on interannual variability in the Nordic Arctic compared to the circum-Arctic. *Permafrost and Periglacial Processes*, *32*(1), 47–58.
Strunk, A., Larsen, N. K., Nilsson, A., Seidenkrantz, M.-S., Levy, L. B., Olsen, J., & Lauridsen, T. L. (2018). Relative sea-level changes and ice sheet history in Finderup Land, North Greenland. *Frontiers of Earth Science*, *6*, 129.
Strunk, A., Olsen, J., Sanei, H., Rudra, A., & Larsen, N. K. (2020). Improving the reliability of bulk sediment radiocarbon dating. *Quaternary Science Reviews*, *242*, 106442.
Sturm, M., Holmgren, J., & Liston, G. E. (1995). A seasonal snow cover classification system for local to global applications. *Journal of Climate*, *8*(5), 1261–1283.
Svennevig, K. (2018). Update of the seamless 1: 500 000 scale geological map of Greenland based on recent field work in the Wandel Sea basin, eastern North Greenland. *Geological Survey of Denmark and Greenland Bulletin*, 39–42.
Throop, J., Lewkowicz, A. G., & Smith, S. L. (2012). Climate and ground temperature relations at sites across the continuous and discontinuous permafrost zones, northern Canada. *Canadian Journal of Earth Sciences*, *49*(8), 865–876.

Van Nieuwenhove, N., Limoges, A., Nørgaard-Pedersen, N., Seidenkrantz, M.-S., & Ribeiro, S. (2020). Episodic atlantic water inflow into the independence fjord system (eastern North Greenland) during the Holocene and last glacial period. *Frontiers of Earth Science*, *8*, 405.

Westermann, S., Elberling, B., Højlund Pedersen, S., Stendel, M., Hansen, B. U., & Liston, G. E. (2015). Future permafrost conditions along environmental gradients in Zackenberg, Greenland. *The Cryosphere*, *9*(2).

Wu, Y., Nakagawa, S., Kneafsey, T. J., Dafflon, B., & Hubbard, S. (2017). Electrical and seismic response of saline permafrost soil during freeze-thaw transition. *Journal of Applied Geophysics*, *146*, 16–26.